Groundstate and finitetemperature energetics and topologies of germanium microclusters

Giomal A. Antonio, Bradley P. Feuston, Rajiv K. Kalia, and P. Vashishta

Citation: The Journal of Chemical Physics **88**, 7671 (1988); doi: 10.1063/1.454281
View online: http://dx.doi.org/10.1063/1.454281
View Table of Contents: http://scitation.aip.org/content/aip/journal/jcp/88/12?ver=pdfcov
Published by the AIP Publishing

Ground-state and finite-temperature energetics and topologies of germanium microclusters[a)]

Giomal A. Antonio
Departamento de Fisica e Ciência dos Materiais, Instituto de Fisica e Química de São Carlos, Universidade de São Paulo 13560-São Carlos, SP, Brasil and Materials Science Division, Argonne National Laboratory, Argonne, Illinois 60439

Bradley P. Feuston
Department of Ceramics, Rutgers University, Piscataway, New Jersey 08855

Rajiv K. Kalia and P. Vashishta
Materials Science Division, Argonne National Laboratory, Argonne, Illinois 60439

(Received 22 September 1987; accepted 11 March 1988)

We have investigated the ground-state and finite-temperature properties of Ge microclusters ($N = 2$ to 14) using molecular dynamics (MD) simulation along with the method of steepest-descent quench (SDQ). The interaction potential adopted is the three-body Stillinger–Weber potential as modified by Ding and Andersen for amorphous Ge. Our results indicate that the experimentally observed greater stability of certain cluster sizes can be explained by the topology and energetics of the clusters at finite temperature rather than by the binding energies of the ground-state structures.

I. INTRODUCTION

In the past few years, microclusters of Group IV elements, particularly Si and Ge, have been intensively studied due to their scientific and technological applications. In a recent photofragmentation study of Si microclusters by Bloomfield, Freeman, and Brown,[1] a pulsed beam of neutral clusters ($N = 2$ to 12) was ionized and separated by time of flight techniques. The measurements of relative abundance of cluster sizes pointed out that Si_6 and Si_{10} were the most prominent species after fragmentation. Using the same technique, Heath *et al.*[2] performed ionization studies on Si and Ge using lasers of different energies, and observed that the fragmentation patterns for both elements were remarkably similar, showing a marked tendency to fragment by fission into small clusters of 6–11 atoms. Their results indicate particularly strong peaks at $N = 6$ and 10. In another experiment, Martin and Schaber[3] produced clusters by thermal evaporation followed by quenching in a He gas atmosphere and ionized by electron beam scattering (70 eV). The clusters were analyzed by a quadrupole mass spectrometer, and the mass spectrum for Ge showed highly stable clusters of 6, 10, 14, 15, and 18 atoms. More recently, Phillips[4] presented the data of Bloomfield and co-workers on Ge showing that 6 and 10 atoms microclusters are the most abundant from fragmentation of larger clusters.

To explain the relative stabilities of certain clusters sizes, several models and theoretical calculations have been proposed. Bloomfield *et al.*[1] constructed a geometric model in which the essential structures are the reconstructed six-membered "chair" ring and the "adamantane cage" formed by the ten-membered microcrystal subunit of the tetrahedral diamond lattice. This model accounts for the photofragmentation data since both geometries are tightly bound and therefore more stable. The geometries for other sizes can be constructed by adding atoms to these basic structures.

Based on the fact that crystalline and amorphous Si are tetrahedrally bound, Martin and Schaber[3] proposed a model where the basic units are Si atoms connected with four others (Si or H) and the bond angle is around 109° with deviations of less than 1°. Their structural units are the six-membered rings in the form of a boat or chair and five-membered rings in the form of planar pentagons. The structures of larger microclusters are different combinations of the five- and six-membered rings.

Saito, Ohnishi and Sugano[5] introduced a model potential for the interaction between atoms in which the repulsive term is a Yukawa's potential and the attractive part is formed by four "attractive centers" around each atom forming a tetrahedron with the restriction that if the ith atom sits on one of the attractive centers of the jth atom, the jth atom also sits on one of the attractive centers of the ith atom. With this potential they calculated the stable structures of Group IV microclusters with 2–20 atoms, minimizing the total energy by the quasi-Newton method. They found that the isosceles triangle, "flattened" tetrahedron, and the regular pentagon are the most stable structures for $N = 3$, 4, and 5, respectively. For $N \geqslant 6$ they determined two sets of lowest-energy configurations: one formed only by six-membered rings and other one formed mainly by four- and five-membered rings. The former was called the "crystalline series" because of the similarity of the radial distribution function (RDF) of this series with that of the diamond lattice. The latter was called the "amorphous series" because, like in the experimental RDF for amorphous Ge (Ref. 6) the RDF of the dodecahedron, which is the stable configuration for $N = 20$, does not have the third peak at 4.71 Å, characteristic of the crystalline phase. Based on relatively high binding

[a)] Work supported in part by the U. S. Department of Energy, BES-Materials Sciences, under Contract No. W-31-109-ENG-38.

 0021-9606/88/127671-16$02.10

energies per atom, Saito *et al.*[5] determined the magic numbers to be $N = 6$, 10, 14, and 18, for the crystalline series and $N = 5$, 10, 12, 16, 18, and 20 for the amorphous series. The structures of larger clusters are formed basically by adding a corner-shared atom or edge-sharing rings to the $N = 5$ cluster configuration.

The stability of Si and Ge clusters containing 3–7 atoms at $T = 0$ was investigated by Pacchioni and Koutecky[7] using the pseudopotential molecular orbital-linear combination of atomic orbitals (MO-LCAO) method followed by the configuration interaction procedure. Among several structures considered for each cluster, they found that the isosceles triangle and the linear Ge_3 have nearly the same stability and are slightly more stable than the equilaterial triangle. The planar geometries for Ge_4 (rhombus and square) are preferred over more compact structures like the tetrahedron. Also the Ge_4 chain structure was found to spontaneously dissociate into dimers. The lowest energy structure for Ge_5 was the trigonal bipyramid (but they did not consider the regular pentagon as a possible structure). The three closed-packed Ge_6 structures, tripyramid, octahedron, and pentagonal pyramid, are much more stable than the planar hexagon and the hexagonal chair, which is a section of the crystalline structure. As a general result they found that Si and Ge microclusters have very similar electronic structures and although some planar structures possess considerable stability, the compact structures are more favorable than the linear ones.

Detailed quantum mechanical calculation on small Si clusters were performed by Raghavachari and Logovinsky[8] and Tomanek and Schlüter.[9] Recent reviews by Phillipps[10] and Brown *et al.*[11] give an insight into state-of-the-art calculations on covalently bonded clusters.

Another approach used in the study of small clusters is the computer simulation by the molecular dynamics (MD) method. This approach needs an effective potential for the interaction between particles. For covalently bonded monoatomic systems such as Si and Ge the Keating[12] potential has been used for nearly two decades. Recently several effective potentials have been proposed, the Stillinger and Weber[13] (SW) three-body potential, the Tersoff potential,[14] which is a Morse-type potential with the bond strength parameter determined by the local environment, the Pearson *et al.*[15] potential and the Biswas–Hamann[16] potential.

Using the Stillinger–Weber potential Barojas and Levesque[17] considered both neutral and positively charged Si clusters. They determined through the MD method the minimum energy configurations by an annealing process. Using MD with the steepest-descent quench (SDQ) method, Feuston *et al.*[18] have determined the ground-state structures, the high-temperature configurations, and the energetics of the fragmentation process in Si microclusters. The advantage of using MD with SDQ rather than simple MD annealing is that the SDQ method allows an infinitely fast quench, driving the system to the nearest configuration where the force and velocity of each particle vanish. In the case of MD quench, sometimes one may obtain a system which is trapped in a shallow minimum which is above the global minimum and due to the very low temperatures or small velocities of particles is unable to make a transition to the global minimum. Performing SDQ instead of molecular dynamics quench allows a much more reliable mapping of the energy hypersurface.

Small clusters of Si ($N = 4$ and 5) were also studied by Car, Parrinello, and Andreoni[19] through the novel technique of simulated annealing. In this technique, developed by Car and Parrinello,[20] the interatomic interactions are treated on the level of density-functional theory[21] (DF) and a fictitious time dependence of the electronic orbitals is introduced in order to compose a classical Lagrangian for the system. Through a MD calculation with an annealing process one gets the equilibrium configuration of the fictitious system, which corresponds to the electronic ground state of the real system.

Recently, Ding and Andersen[22] (DA) investigated the properties of amorphous Ge using the SW potential, but adjusting the parameters to fit the cohesive energy, density, and elastic constants of the crystalline Ge. Using these parameters, they calculated the phonon dispersion curves for crystalline germanium and the agreement with experiment was found to be good.

The purpose of this work is to investigate the ground-state and finite-temperature properties of Ge clusters in the range $N = 2$–14, considering the DA modification of the Stillinger-Weber potential. The procedure is the same as that used by Feuston *et al.*[18] to obtain results for Si microclusters: through the MD technique we study the temporal evolution of the systems and through the SDQ method we find the underlying mechanically stable structures at finite temperatures.

In Sec. II, we will give a general description of the interaction potential and a brief discussion about the MD and SDQ methods. In Sec. III, we discuss the ground-state structures and compare them with the previous results on Si. Section IV contains the analysis of the clusters at finite temperature considering their most frequent structures. The calculation of the pair-distribution-function $g(r)$ at low temperatures is given in Sec. V. Section VI contains a discussion of the fragmentation process.

II. INTERACTION POTENTIAL AND METHODS

A. Interaction potential

The functional form of the Ding and Andersen[22] potential is the same as the Stillinger–Weber[13] potential for Si. It is a sum of a two-body potential and a three-body interaction term. The two-body term, in reduced units, has the form

$$V_2 = \begin{cases} A(Br^{-p} - r^{-q})\exp[(r-a)^{-1}], & r < a \\ 0, & r > a \end{cases}, \quad (1)$$

where "a" sets the range of the potential, B is adjusted so that the minimum in the potential corresponds to the cohesive energy of the crystal, and A is chosen so that the value of V_2 at the minimum is -1.

The three-body term introduces a bond-bending force which favors tetrahedral angles. It is given by

$$V_3 = h(r_{ji}, r_{ki}, \theta_{jik}) + h(r_{kj}, r_{ij}, \theta_{ijk}) + h(r_{jk}, r_{ik}, \theta_{ikj}), \quad (2)$$

where

$$h(r_{ji},r_{ki},\theta_{jik}) = \sum_{i<j<k} \lambda \exp\{\gamma[(r_{ji}-a)^{-1} + (r_{ki}-a)^{-1}]\}(\cos\theta_{jik}+1/3)^2, \quad (3)$$

provided that both r_{ji} and r_{ki} are smaller than a. Otherwise $h=0$. This functional form guarantees that the potential and its derivatives approach zero continuously when the cutoff distance a is reached.

In order to determine the various parameters in the potential, Ding and Andersen[22] used the experimental data on crystalline Ge with the diamond structure as having the lowest energy. The depth of the two-body potential was fitted to the cohesive energy of the crystal at 0 K and the location of the minimum was determined by the density of the crystal at a pressure of 1 atm. The three elastic constants C_{11}, C_{12}, and C_{44} of the crystal were used in selecting other parameters. The remaining parameters were obtained through a comparison of the calculated radial distribution function in the amorphous solid with the experimental results. With the optimum choice of the parameters the phonon dispersion curves for crystalline Ge were calculated and found to be in good agreement with the experiment.

The values of A, B, p, q, λ, γ, and a, and the energy and length scales, ϵ and σ, for Ge are given on Table I. Comparing these with the values for Si we see that, besides the changes in the energy and length scales the main difference is in the strength of the three-body interaction: $\lambda = 21$ for Si and 31 for Ge. This change is expected to affect those structures for which the three-body interaction contributes significantly.

B. Molecular dynamics (MD)

Molecular dynamics is a useful computer simulation technique in the study of classical systems for which the interaction potential between particles is known. In a conventional MD calculation an infinite system is simulated by placing $N \approx 500$–5000 particles in a cell of fixed volume and using periodic boundary conditions to remove surface effects in a controlled manner. The total energy, the number of particles and the volume are usually the conserved quantities (E, N, Ω ensemble). The temporal evolution of the system is determined by the integration of the equations of motion using an appropriate algorithm and the temperature is given by the average kinetic energy of the system. By scaling the velocities it is possible to heat or cool the system.

Since the clusters are finite systems, it is not necessary to use periodic boundary conditions. For each N-atoms cluster, we used as a starting point a configuration with positions and velocities distributed in such a way that both linear and angular momenta are zero. The temporal evolution of the system was determined by integrating the equations of motion using Beeman's algorithm.[23] In this method the positions and velocities at time $t+\Delta t$ are given by

$$x(t+\Delta t) = x(t) + v(t)\Delta t + [4a(t) - a(t-\Delta t)](\Delta t)^2/6, \quad (4)$$

$$v(t+\Delta t) = v(t) + [2a(t+\Delta t) + 5a(t) - a(t-\Delta t)]\Delta t/6, \quad (5)$$

where $a(t)$ is the acceleration calculated from the forces. The equations of motion were integrated by using a time step $\Delta t = 6.8\times10^{-16}$ s. The accuracy of the calculation was monitored through the total energy of the system which is conserved to 1 part in 10^4 over thousands of time steps.

As is usual in MD calculations we worked with reduced units: ϵ and σ are units of energy and length, respectively. The reduced temperature T^* is defined by

$$T^* = k_B T/\epsilon, \quad (6)$$

where k_B is the Boltzmann constant. The room temperature (300 K) in reduced units is $T^* = 0.013$.

Systems with higher (or lower) energies were generated by increasing (or decreasing) the velocities of all the particles by a factor f defined by

$$f = \sqrt{T_R/T}, \quad (7)$$

where T_R is the required new temperature and T is the temperature of the system before heating or cooling. Following each scaling, the system was thermalized for several thousand time steps and then the averages of the quantities of interest were evaluated.

C. Steepest-descent quench (SDQ)

The motion of a N-particle system interacting through a potential $V(R)$, $R(t) = [r_1(t), r_2(t), \ldots, r_N(t)]$, can be analyzed in terms of vibrations (possibly anharmonic) around minima on the $3N$-dimensional surface defined by the potential $V(R)$. From this point of view one can associate uniquely a minimum with each configuration of the N particles through the steepest possible path.

When the system is in equilibrium, the MD trajectory can be thought as a set of successive configurations at the same energy. In order to find the underlying local minimum at a given time one needs to remove all the kinetic energy from the system and drive it to a configuration where the net force on each particle vanishes. The ideal method to achieve this is the steepest-descent method (SDQ), which corresponds to an infinitely rapid quench. The SDQ involves solving the differential equation,

$$\frac{\partial R}{\partial s} = -\nabla_R V(R) \quad (8)$$

in the limit $s\to\infty$ and the solution corresponds to $\nabla_R V(R) = 0$, i.e., the zero force configuration. This equation connects by the steepest-descent path each point $R(t)$ in the MD trajectory to a local minimum on the potential-energy hypersurface. The actual implementation of the steepest-descent quench was done by the conjugate-gradient method, an efficient numerical method to find the minimum of a function of many variables.

At very low temperatures the SDQ mapping will always give the same minimum if the system does not have enough

TABLE I. Potential parameters for Ge, as found by Ding and Andersen (Ref. 22).

$A = 7.049\,556\,277$	$q = 0$	$a = 1.8$
$B = 0.602\,224\,5584$	$p = 4$	$\gamma = 1.2$
$\epsilon = 3.085\times10^{-12}$ ergs	$\sigma = 2.181$ Å	$\lambda = 31$

energy to overcome the potential barrier between two minima. But, as the temperature increases, more and more local minima will be accessible. In this case, a SDQ mapping at different times will give a collection of different local minima. So, through a detailed search, it is possible, in principle, to determine the global minimum on the potential energy hypersurface. Therefore, MD in conjunction with SDQ provides a useful tool in the study of the underlying mechanically stable structures at finite temperatures.

III. GROUND-STATE STRUCTURES

Let us investigate the ground-state structure for each cluster size. As we pointed out in the previous section, this can be achieved by a detailed search of the minima in the configurational space. In order to do this efficiently we have to have the systems at sufficiently high temperatures so that in the $6N$-dimensional phase space the system is able to sample various potential energy minima.

The initial configuration for each of these systems was taken to be the fragments of the diamond structure. For small clusters ($N = 2$–9), these initial configurations were found to be stable, but were not the lowest-energy configuration. For larger clusters, $N > 9$, the diamond fragments were unstable and cluster configurations of lower energy were attained by the method of steepest descent and these were used as the starting configurations. From the above initial configurations, after setting random velocities to the particles, we increased the temperature by scaling the velocities by a factor of 1.2 for systems below room temperature and 1.1 for those heated above room temperature. After scaling the velocities each system was relaxed for 2000 time steps.

In order to find the different local minima accessible for each cluster size, a set of ten systems at temperatures above the room temperature were chosen and for each one, we performed a 10 000 Δt MD run in which a SDQ mapping was done at every 100 Δt. Repeating this procedure, we located 1000 underlying minima in the configurational space of each cluster size. Most of the minima are structurally the same and in a few cases there are different structures with degenerate energies. For example, structures with reduced energy $-(N-1)/N$ are a special case in which the three-body term is zero (tetrahedral angles) and for each pair of particles the two-body potential energy is -1 (the distance between them is the nearest-neighbor distance in the crystal). So, any combination of $N-1$ bonds maintaining the tetrahedral angle has that energy. Specifically, for $N = 5$, the tetrahedron and the chain have the same energy.

Analyzing the set of distinct structures we find the one with the lowest energy and regard it as the ground state. Comparing these structures with those for Si microclusters we note that despite many similarities there are some significant differences, which we will point out. Figure 1 shows the ground-state structures of various clusters sizes.

(i) $N = 2$: The dimer is a trivial case in which, as expected by the construction of the interaction potential, the distance between the two atoms is 1.12σ, corresponding to the nearest-neighbor distance in the crystalline germanium.

(ii) $N = 3$: The isosceles triangle with only two bonds forming a tetrahedral angle is the ground-state structure for

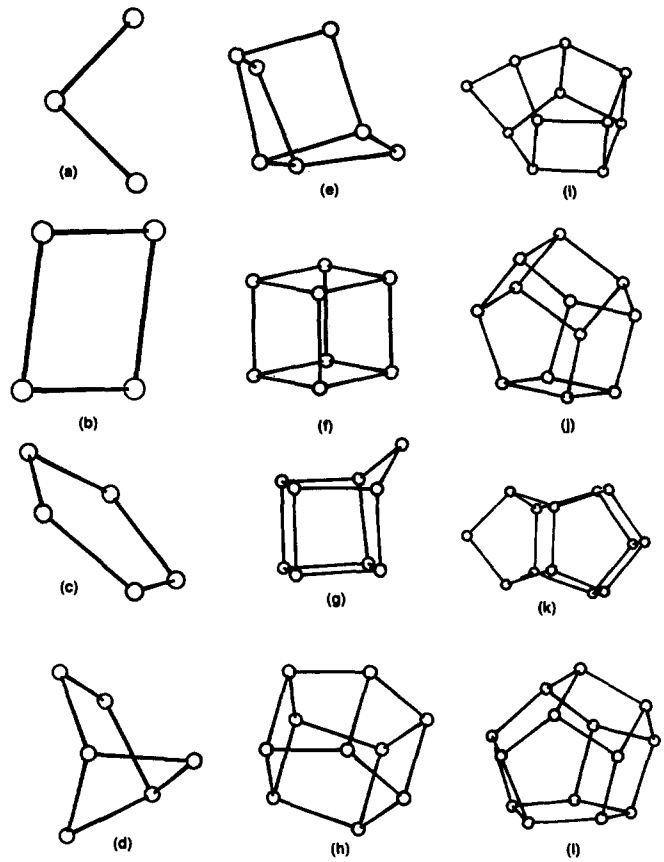

FIG. 1. Ground state structures for Ge_N, $N = 3$ to 14. The energy per atom on each structure is given in units of ϵ(= 1.93 eV): (a) $E(3) = -0.6667$, (b) $E(4) = -0.9064$, (c) $E(5) = -0.9995$, (d) $E = -1.0466$, (e) $E(7) = -1.1265$, (f) $E(8) = -1.2402$, (g) $E(9) = -1.2710$, (h) $E(10) = -1.3208$, (i) $E(11) = -1.3414$, (j) $E(12) = -1.3764$, (k) $E(13) = -1.3894$, and (l) $E(14) = -1.4168$.

Ge_3. The difference from Si, where the equilateral triangle had the lowest energy, can be understood as a direct consequence of increasing the strength of the three-body interaction. The energy gained from an extra bond is lost because of the three positive contributions from the three-body term. The present result agrees well with the quantum-mechanical calculation[7] and is also found in the model of Saito *et al.*[5]

(iii) $N = 4$: In this case the ground-state structure is a square, which can be formed by edge capping one atom to the open side of Ge_3. The principal feature in the square is the existence of repulsive forces due to the three-body interaction. In the quantum-mechanical calculation,[7] the rhombus and the square have nearly the same stability, while the model of Saito *et al.*[5] gives a flattened tetrahedron as the lowest-energy structure.

(iv) $N = 5$: A regular pentagon can be constructed by relaxing an edge-capped square. The small deviation from the tetrahedral angle reduces the influence of the three-body term which makes this structure most prominent in the formation of larger clusters.

The pentagonal structure is also found in the model of Saito *et al.*[5] but in the work of Pacchioni *et al.*[7] a squashed trigonal bipyramid is the more stable configuration.

(v) $N = 6$: The ground-state structure for Ge_6 is a reconstructed face-capped pentagon and it is the first three-dimensional configuration to appear. This structure is very compact in that all the second nearest-neighbor distances are shorter than the range of the potential. This structure is significantly different from the one for Si, where the ground state is constructed by two stacked equilateral triangles forming a wedge. In the case of Ge, the wedge will have a very high energy due to a large three-body contribution in the equilateral triangle. Pachioni *et al.*[7] find that the closed-packed configurations for Ge_6 are preferred over the crystalline fragment (six-membered ring chair). The structure predicted by Saito *et al.*[5] is a corner-capped pentagon. We find the energy of the corner-capped pentagon to be slightly greater than that of the face-capped pentagon, although as we shall see the former is a very common structure at finite temperatures.

(vi) $N = 7$: The ground-state configuration of Ge_7 is a trigonal pyramid in which three atoms are edge capped to each side of its base. The quantum-mechanical calculation considers only a pentagonal bipyramid for Ge_7. Saito *et al.*[5] find a square joined to a pentagon across an edge. We find that the energy of this structure is 3% greater than the ground-state configuration.

(vii) $N = 8$: The ground-state structure is a perfect cube. It can be obtained by attaching an atom to the open corner of Ge_7. In this symmetric structure all the atoms contribute equally to the final energy of the system. The effect of the three-body interaction is manifested in the slight increase (4%) in the nearest-neighbor distance ($1.17\,\sigma$) over that in the crystalline one.

Hitherto no quantum mechanical calculation for Ge clusters with more than seven atoms has been performed because of the large number of possible configurations, which increases the cost of these calculation enormously. The structure predicted by Saito *et al.*[5] consists of two edge-sharing pentagons, which in our case has an energy 10% greater than that of the cube.

(viii) $N = 9$: The ground state for Ge_9 is obtained by edge capping one atom to one side of the cube and allowing the structure to relax. The stable structure found by Saito *et al.*[5] is composed of two pentagons and a square edge sharing two sides and forming an open structure with five twofold coordinated atoms.

(ix) $N = 10$: The two stacked pentagons can be obtained by the same process of edge capping one atom to the $N-1$ structure followed by relaxation. In this structure, although all atoms contribute equally, as in the case of Ge_8, the nearest-neighbor distance is very close to that in the crystalline phase, because in the pentagons the three-body term is very small. Saito *et al.*[5] found three edge-sharing pentagons, which is much less compact than two stacked pentagons.

(x) $N = 11$: This structure can be built from Ge_{10} by inserting one atom between the stacks. It is different from the ground state for Si which was constructed by face-capping one atom to the pentagon thus forming a structure with a fourfold coordinated atom. One can explain this in terms of the competition between the tendency of the system to maximize the number of bonds and simultaneously minimize the effect of the three-body interaction. For Si it is preferable to form two extra bonds and have a fourfold coordinated atom which has a large three-body. Since the three-body term is stronger for Ge, the system gains energy by forming only one extra bond but reducing the above interaction by forming a twofold coordinated atom.

(xi) $N = 12$: A basic characteristic of even clusters with $N > 6$ is that they have all the atoms threefold coordinated and therefore very symmetric. The structure for Ge_{12} can be formed by capping one atom to the face of one pentagon with the twofold coordinated atom in Ge_{11} and relaxing the structure.

(xii) $N = 13$: The structure for Ge_{13} can be built by edge capping the single bound atoms of the Ge_3 to two adjacent stacks on the Ge_{10} configuration, the two stacked pentagons. This structure is also different from the ground state for Si_{13} which has a fourfold coordinated atom. The explanation given above for Ge_{11} also applies to Ge_{13}.

(xiii) $N = 14$: Again, we have a very symmetric structure composed of six pentagons and three squares with all the threefold coordinated atoms distributed spherically.

Since the contribution of the three-body term is always positive, increasing its strength increases the energy of the system. This can be observed in Fig. 2, where we compare the ground-state energies of Ge [$\lambda = 31$, Eq. (3)] with those for Si ($\lambda = 21$). Note that: (a) the smallest difference occurs for $N = 5$ since the distortion from the tetrahedral angle is very small for a regular pentagon, and (b) the largest difference occurs for $N = 8$, the perfect cube, where all the atoms are threefold coordinated and all the angles are 90° causing a very large contribution to the three-body term.

The stable structures predicted by Saito *et al.*[5] at $T = 0$ K for $N = 6$, 7, 8, and 11 are in general open structures and we find these open structures only at finite temperatures, where entropy and thermally induced expansion transform the $T = 0$ structures.

In previous work on clusters, the presence of magic numbers has always been associated with the relatively high binding energies calculated for the ground-state structures.

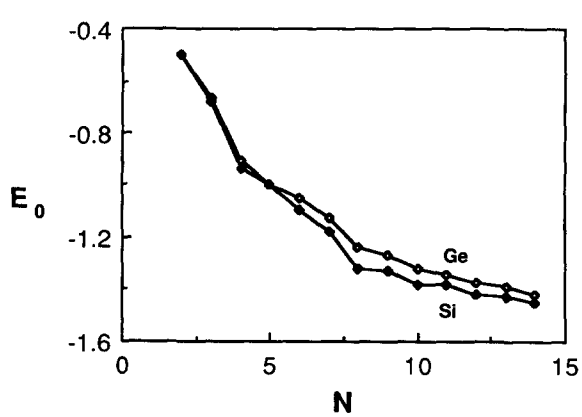

FIG. 2. Comparison between the ground-state energies for Ge and Si. The largest difference occurs for the cube ($N = 8$) and the smallest for the pentagon ($N = 5$). Recall that in reduced units the only difference between Ge and Si is in the strength of the three-body interaction.

Our results do not indicate a firm relationship between the ground-state energies and the expected magic numbers observed in the fragmentation spectra at high temperature.

Experimental results suggest that fragmentation occurs at temperatures of the order of the bulk melting temperature. At such high temperatures it is improbable that the system remains in the ground state. As we shall see, at high temperatures there are other more probable configurations than those corresponding to the ground state. Therefore, to understand cluster dissociation one should investigate the finite-temperature structures.

IV. CLUSTERS AT FINITE TEMPERATURES

In the process of finding the ground state, we observed, for each cluster, a set of underlying structures with different energies corresponding to local minima on the potential energy hypersurface. The number of these structures increases with the cluster size; for $N = 14$ more than 150 distinct configurations were identified. Since it is not possible to investigate every structure for each different value of N, we chose to analyze those that are statistically important in the fragmentation process.

Fragmentation implies a situation in which the separation of an atom or a group of atoms from the remaining cluster is greater than the range of the interaction potential. The fragmentation energy (E_f) is then the lowest energy at which a system fragments on a macroscopic time scale. However, in MD calculations we adopt a practical definition, namely the highest energy where the system remains bound for over 25 000 Δt. The fragmentation temperature T_f is then the temperature of the system with energy E_f.

The principal objective of this study is to determine E_f and T_f for each cluster and also investigate the distribution of underlying mechanically stable structures visited by the system at different temperatures.

Starting from the ground-state structure we heat the system monotonically. After heating, the system is thermalized for 1000 Δt and then a 11 000 Δt MD run is made in

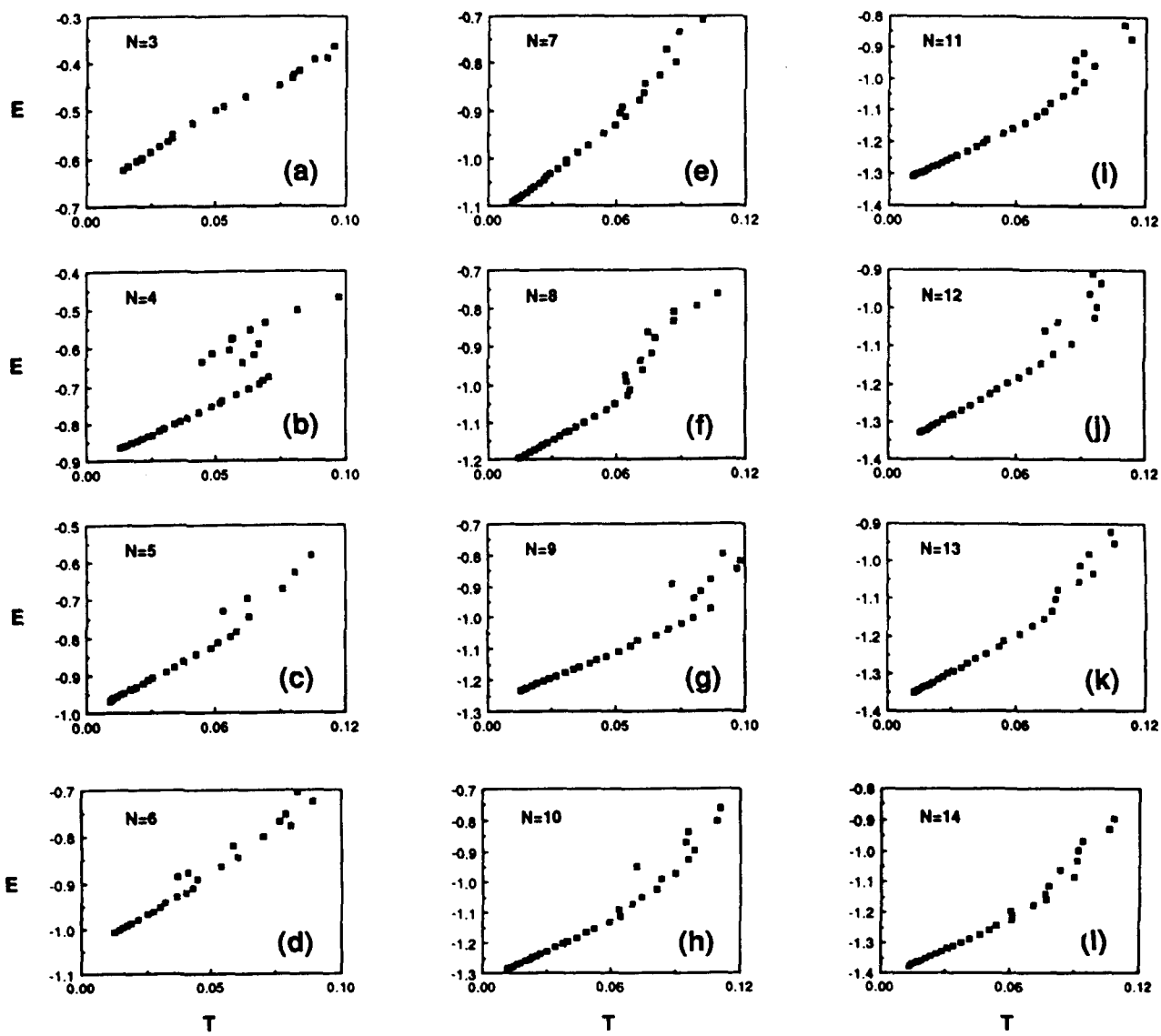

FIG. 3. Energy vs temperature curves for Ge clusters with $N = 3$–14 atoms. The fluctuations in the temperature at high energies indicate the changes in the underlying structure of the clusters. All of them were heated from the ground state at $T = 0$.

order to get the temperature. We generate about 30 equilibrium ensembles below the fragmentation temperature. Figure 3 shows the curves E vs T for each cluster size obtained by the above process. The interesting feature in this figure is the large temperature variation at high energies arising from transformations that a system undergoes among different structures.

After determining the fragmentation energy E_f (discussed below in Sec. VI) we perform a 5000 Δt MD run along with SDQ at intervals of 5 Δt on systems whose energies are around 0.25 E, 0.50 E, 0.75 E, and 0.95 E where E is the fragmentation energy relative to the ground-state energy. This gives a broad distribution of underlying structures for each cluster. At 0.25 E, for most clusters, the SDQ mappings give the ground state as the only available structure. However at higher energies the system undergoes structural changes. This is a general feature independent of the detailed nature of the ground-state structure or the number of particles in the cluster. Figure 4 shows the distribution of energies for the inherent structures at 0.95 E for each cluster size. Below we discuss the results of each of these calculations.

(i) $N = 3$: The direct consequence of increasing the strength of the three-body term in the SW potential from $\lambda = 21$ to $\lambda = 31$ is that the ground-state configuration of Ge_3 is an isosceles triangle with two bonds forming a perfect tetrahedral angle [Fig. 5(a)]. The energy of an equilateral triangle [Fig. 5(b)] is 12% greater than that of the ground state. So the increase in energy resulting from the third bond makes this structure rare even at high temperatures. The equilaterial triangle occurs only 3.5% of the time at 0.50 E and near the fragmentation its occurrence decreases to 1%.

(ii) $N = 4$: There are four structures and two of these structures are degenerate in energy. In order of increasing energies we have the square [Fig. 1(b)], the chain [Fig. 6(a)], the trigonal pyramid [Fig. 6(b)], and the corner-capped triangle [Fig. 6(c)]. The chain and the trigonal pyramid are degenerate in energy since both have three bonds and all the angles are tetrahedral so that there is no contribution from the three-body term. Again, the structure with the highest energy, the corner-capped triangle, is visited less frequently than the other structures. *Close to the fragmentation temperature the dominant* ($\approx$75%) *underlying structure is the chain.* This can explain why the most common channel of fragmentation for Ge_4 is to dimers instead of the $N \rightarrow (N-1) + 1$ channel which is usually the case for other clusters.

The distribution of underlying structures can also explain the large fluctuation in temperature [Fig. 3(b)] observed for this cluster. As the two most commonly visited structures, the chain and the square, differ by the largest amount of energy [0.15 ϵ in Fig. 4(b)] among all cluster sizes, the change from one structure to another gives rise to the largest fluctuation in the kinetic energy.

(iii) $N = 5$: Although there are eight possible configu-

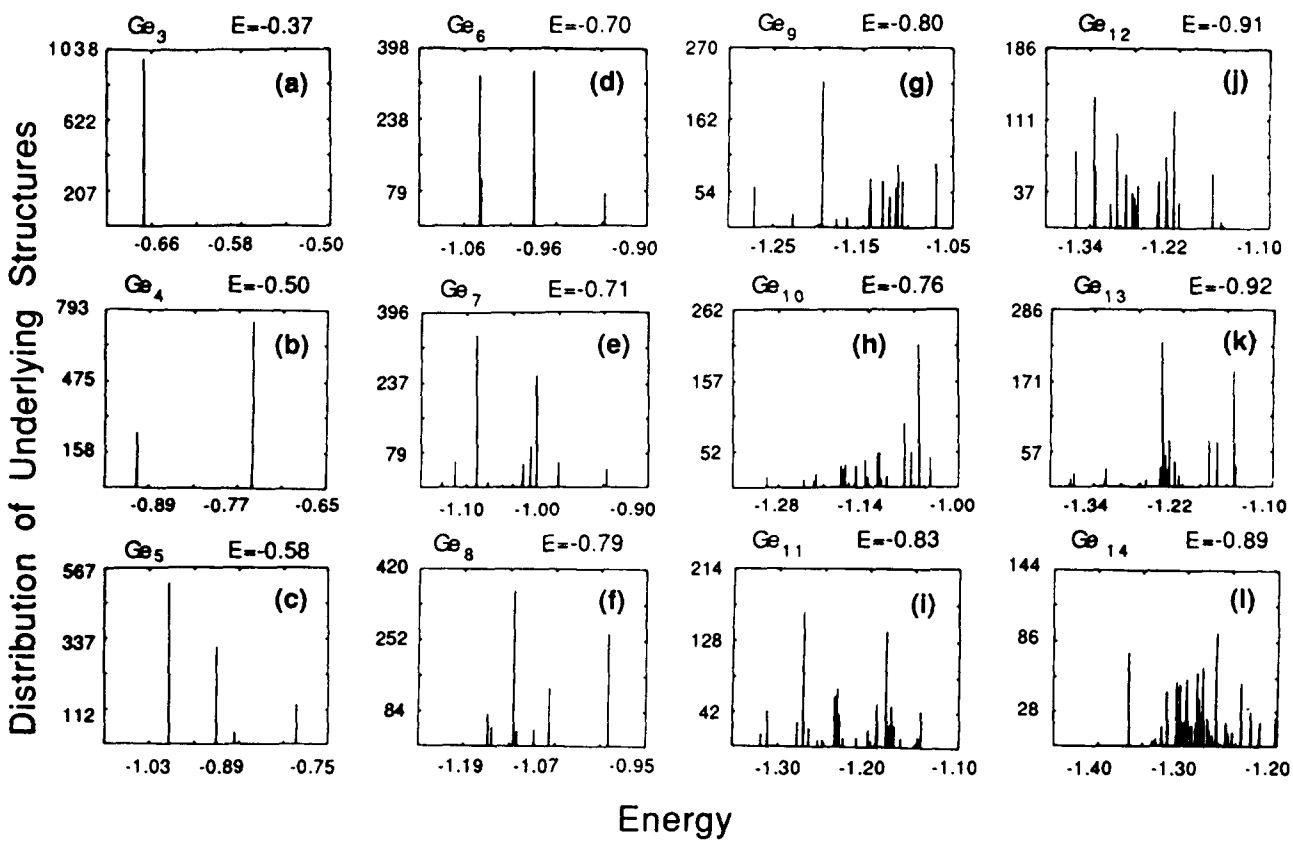

FIG. 4. Distribution of underlying structures at energies near fragmentation (0.95 E) for Ge clusters with $N = 3$–14 atoms. Each histogram is the result from 1000 SDQ mappings executed during a MD run of 5000 Δt. The indicated energy on the top of each graphic is to be related with the corresponding curve in Fig. 3 in order to identify the starting system for this calculation.

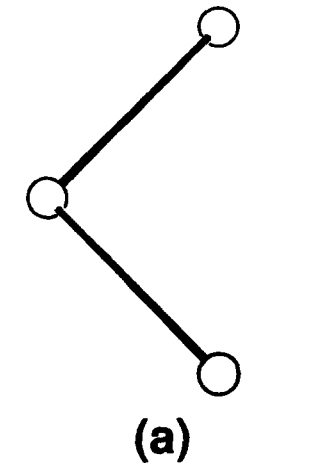

FIG. 5. Ge_3 structures at finite temperatures. (a) Ground state, isosceles triangle with two bonds forming a perfect tetrahedral angle, $E = -0.6667$; (b) equilateral triangle, $E = -0.5893$.

rations for Ge_5, only five of them are visited frequently at finite temperatures. In order of increasing energies, they are the regular pentagon [Fig. 1(c)], the corner-capped square [Fig. 7(a)], the squashed trigonal bipyramid [Fig. 7(b)], the chain [Fig. 7(c)], and the capped chain [Fig. 7(d)]. The chains are degenerate in energy since both have four bonds with the tetrahedral angle. They are visited only near

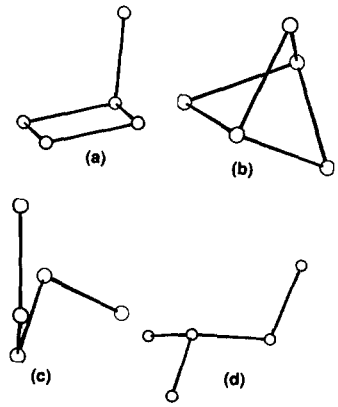

FIG. 7. Ge_5 structures at finite temperatures. (a) Corner-capped square, $E = -0.9251$; (b) trigonal bipyramid, $E = -0.8967$; (c) chain and (d) capped chain, both with the same energy, $E = -0.8000$, since they have four bonds and only tetrahedral angles.

the fragmentation energy. Even at high temperatures the ground state is the most common structure, accounting for 50% of the underlying structures at 0.95 E [Fig. 4(c)].

(iv) $N = 6$: Five different structures have been observed for Ge_6 at high temperatures. In order of increasing energies these are a reconstructed face-capped pentagon [Fig. 1(d)], the two stacked isosceles triangle "book" [Fig. 8(a)], a six membered ring "chair" [Fig. 8(b)], a corner-capped pentagon [Fig. 8(c)], and a chain corner capped to a square [Fig. 8(c)]. The corner-capped pentagon is present 99% of the time at 0.75 E and it is commonly found together with the reconstructed face-capped pentagon at 0.95 E. In the distribution of underlying structures [Fig. 4(d)] we notice the small difference in energy between the reconstructed face-capped pentagon and the two stacked isosceles triangle book. Also the chair and the corner-capped pentagon have nearly the same energy. In order to explain the greater stability of Ge_6, the chair, which is a fragment of the diamond lattice, has been proposed to be the stable structure. We, however find this structure only 13% of the time near the fragmentation temperature.

(v) $N = 7$: Among the 16 structures found for Ge_7 the ground state [Fig. 1(e)] is not the most commonly visited configuration even at low temperatures. At low energies (0.25 and 0.50 E) the predominant structure, an edge-capped book [Fig. 9(a)], has a slightly higher energy than the ground state. All the accessible configurations are visited at 0.95 E, as shown in the histogram of underlying structures

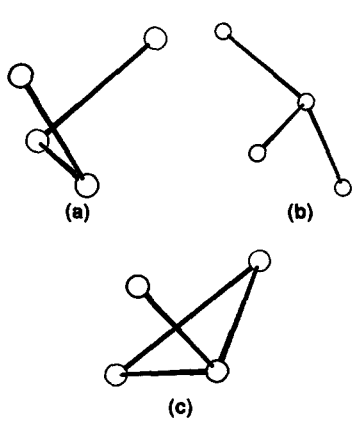

FIG. 6. Ge_4 structures at finite temperatures. (a) The chain and (b) the trigonal pyramid have the same energy, $E = -0.7500$, since they have three bonds keeping the tetrahedral angle between themselves; (c) corner-capped triangle, the structure with the highest energy, $E = -0.6919$.

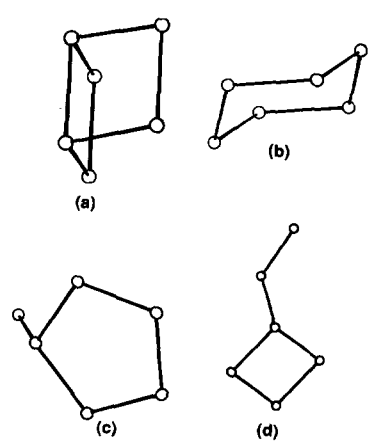

FIG. 8. Ge_6 structures at finite temperatures. (a) Two stacked isosceles triangles book, $E = -1.0453$, whose energy is very close to that of the ground state (-1.0466); (b) six-membered ring chair, $E = -1.0000$, a fragment of the diamond structure; (c) corner-capped pentagon, $E = -0.9995$, the most common structure at high energies and (d) the two atoms chain corner capped to a square, $E = -0.9376$. The energy per atom on each structure is given in units of ϵ (= 1.93 eV).

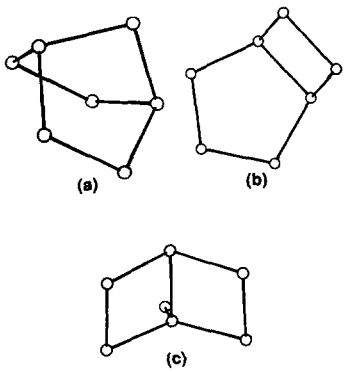

FIG. 9. Ge_7 structures at finite temperatures. (a) Edge-capped book, $E = -1.1209$, the most common structure at low energies; at high energies they are (b) the square edge shared with a pentagon, $E = -1.0899$, and (c) the corner-capped book, $E = -1.0308$.

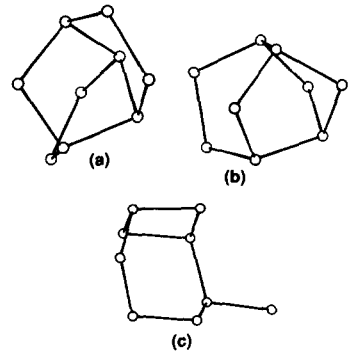

FIG. 11. Ge_9 structures at finite temperatures. The three most frequently visited configurations at 0.95 E: (a) $E = -1.1956$; (b) $E = -1.1955$; and (c) $E = -1.1066$. The structures (a) and (b) differ only in the distribution of the 11 bonds.

[Fig. 4(e)]. The two most common structures at this energy are a square edge shared with a pentagon [Fig. 9(b)] and a corner-capped book [Fig. 9(c)]. The structure in Fig. 9(b) is the most stable zero temperature configuration in the model of Saito *et al.*

(vi) $N = 8$: 23 different underlying structures were found for Ge_8. The three structures showed in Fig. 10 correspond to the peaks in the histogram in Fig. 4(f) and they account for nearly 75% of the underlying structures at high energies. The most common structure [Fig. 10(a)] is also the most stable $T = 0$ configuration in the amorphous series of Saito *et al.* Since the cube is a very compact and symmetric structure with all the atoms threefold coordinated, the system simply oscillates around this ground-state configuration even at 0.50 E.

(vii) $N = 9$: As the cluster size increases, the number of available configurations also increases. But the system does not have a preferred configuration as can be seen in Fig. 4(g) where, with only one exception, each configuration accounts for less than 10% of visitation. At low temperatures the ground state, an edge-capped cube [Fig. 1(g)], is the only available structure; at 0.50 E it is still the dominant structure (50%) whereas at 0.95 E it appears less than 5% of the time. Figure 11 shows the structures corresponding to the three highest peaks in the distribution of underlying structures [Fig. 4(g)].

(viii) $N = 10$: 62 different local minima were found for Ge_{10}, but at 0.50 E only four available configurations are visited. The structure shown in Fig. 12(a) is the most frequent one (55%) at 0.50 E, whereas at 0.75 E this structure appears 35% of the time. At 0.95 E only one configuration appears more than 10% of the time. Figures 12(b) and 12(c) show the most common structures corresponding to two of the highest peaks in the histogram [Fig. 4(h)] at 0.95 E. Breaking one bond in the fourfold coordinated atom in Fig. 12(b) leads to the structure in Fig. 12(c).

(ix) $N = 11$: 50 different configurations were identified for Ge_{11}, although only eight of them are accessible at 0.50 E. In the histogram in Fig. 4(i) we can see that at energies near fragmentation more than 30 different configurations are present, the most common ones occur 15% of the time. The structures corresponding to the three highest peaks in Fig. 4(i) are shown in Fig. 13. The configuration in Fig. 13(c) is the predicted stable configuration at $T = 0$ in the model of Saito *et al.* In our simulations we find several other configurations with lower energy.

(x) $N = 12$: Only 32 distinct structures were identified for Ge_{12}. As the ground-state structure is very compact with all atoms threefold coordinated, the cluster only begins to undergo structural changes at energies above 0.50 E. Near fragmentation the visited structures are distributed uniformly, each appearing less than 15% of the time [Fig. 4(j)]. Figure 14 shows some of the most frequently visited configurations at high energies. Note that the structure in Fig. 14(a) can be constructed by edge capping an atom to the Ge_{11} ground state [Fig. 1(i)].

(xi) $N = 13$: 40 distinct local minima were observed for Ge_{13} and, as shown in the distribution of energies [Fig. 4(k)], only two of them are present more than 15% of the time at high energies. These two structures are shown in Fig. 15. The presence of six-membered rings is not frequent

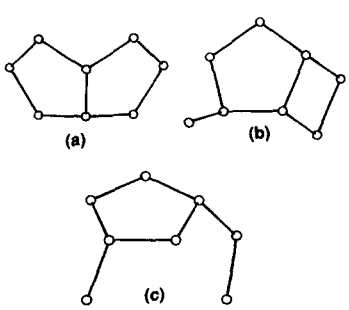

FIG. 10. Ge_8 structures at finite temperatures. The three most frequently visited structures at high energies: (a) two edge-shared pentagons, $E = -1.1243$; (b) corner-capped pentagon edge shared with a square, $E = -1.0778$; and (c) bicorner-capped pentagon, $E = -0.9997$.

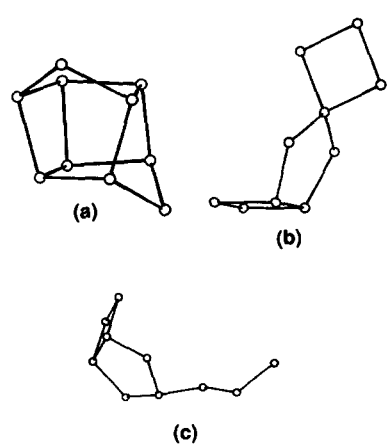

FIG. 12. Ge_{10} structures at finite temperatures. (a) $E = -1.2969$, the most common structure at intermediate energies (0.50 and 0.75 E); (b) $E = -1.1230$; and (c) $E = -1.0623$ are the prominent configurations at energies near fragmentation. Note that (b) can be transformed in (c) by breaking one bond in the fourfold coordinated atom.

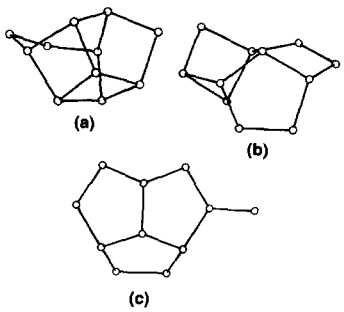

FIG. 13. Ge_{11} structures at finite temperatures. The three most frequently visited configurations at 0.95 E: (a) $E = -1.2722$, (b) $E = -1.2346$, and (c) $E = -1.1811$.

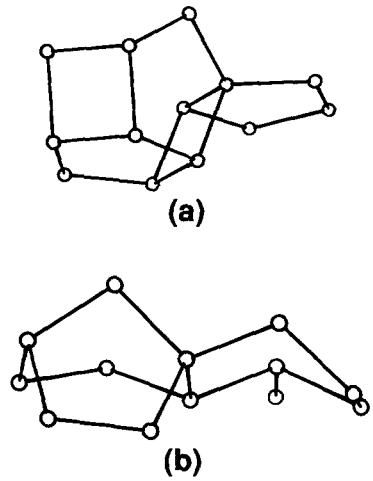

FIG. 15. Ge_{13} structures at finite temperatures. Two of the most common configurations at 0.95 E: (a) $E = -1.2474$ and (b) $E = -1.1503$. The six-membered rings in (b) are not very frequently found.

among the structures examined. Most of them are different arrangements of squares and pentagons, as in Fig. 15(a).

(xii) $N = 14$: 76 structures were found for Ge_{14}, although at 0.50 E the system has access to just three of them. The two structures shown in Fig. 16 account for only 10% of all the visited configurations at 0.95 E. In Fig. 4(l) the distribution of underlying structures shows a marked tendency towards occupying configurations with higher energies.

In Table II we present a list of statistically important structures for Ge clusters with their respective energies obtained after SDQ. To distinguish between structures very close in energy we choose a criterion of $\Delta E \geqslant 1 \times 10^{-4}$ which was suggested by the energy difference ΔE between the chair and the corner-capped pentagon which is equal to 5×10^{-4}. Within this criterion the number of different underlying energies found for each cluster size was 2 for $N = 3$, 4 for $N = 4$, 8 for $N = 5$, 11 for $N = 6$, 16 for $N = 7$, 23 for $N = 8$, 22 for $N = 9$, 62 for $N = 10$, 50 for $N = 11$, 32 for $N = 12$, 40 for $N = 13$, and 76 for $N = 14$. It is important to notice that these numbers were obtained by systematically heating the clusters from their ground state up to temperatures near fragmentation and then performing SDQ on four of these trajectories to determine the underlying mechanically stable structure using the above mentioned criterion for ΔE to distinghish between the structures.

V. PAIR DISTRIBUTION FUNCTION $g(r)$

Recently, with new production techniques, it has become possible to do diffraction experiments on small clusters.[24–26] Small metallic clusters of Ag and Cu were studied by the extended x-ray absorption fine structure (EXAFS) in conjunction with the gas agregation technique.[27,28] Also small rare-gas clusters were investigated by electron diffraction.[29–31] However, there has been no investigation of Ge or Si clusters using these techniques. A quantity that can be obtained from diffraction patterns is the pair-distribution function $g(r)$ which can be easily calculated from the MD trajectories. The pair-distribution function is defined by

$$n(r)dr = 4\pi r^2 \rho g(r) dr, \tag{9}$$

where $n(r)dr$ is the number of particles in a shell of radii r and $r + dr$, and ρ is the number density of the system. Using

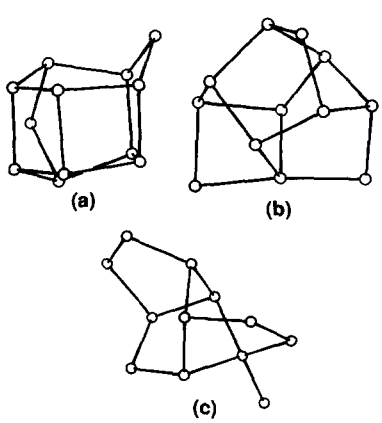

FIG. 14. Ge_{12} structures at finite temperatures. The most prominent structures at high energies: (a) $E = -1.3338$; (b) $E = -1.3033$; and (c) $E = -1.2263$. The energy per atom on each structure is given in units of ϵ ($= 1.93$ eV).

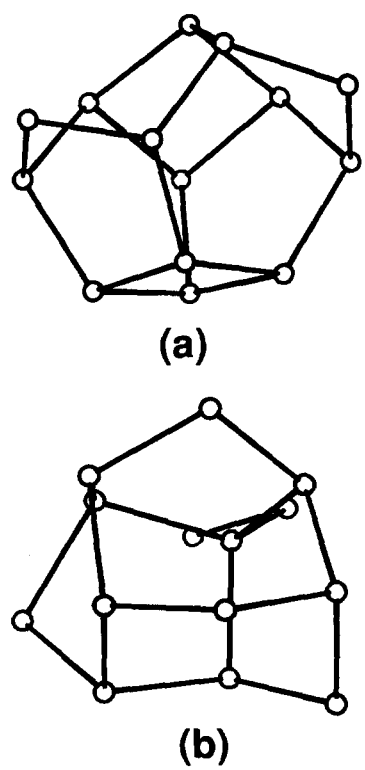

FIG. 16. Ge_{14} structures at finite temperatures. The basic units, pentagons and squares, common to most underlying structures form these most visited configurations: (a) $E = -1.3648$ and (b) $E = -1.2665$.

TABLE II. The most common structures found for each cluster size with their respective energies obtained from SDQ, given in units of ϵ(= 1.93 eV).

N	Structures	Energy
3	Isosceles triangle	− 0.6667
	Equilateral triangle	− 0.5893
4	Square	− 0.9064
	Chain	− 0.7500
	Trigonal pyramid	− 0.7500
	Corner-capped triangle	− 0.6919
5	Pentagon	− 0.9995
	Corner-capped square	− 0.9251
	Trigonal bipyramid	− 0.8967
	Chains	− 0.8000
6	Reconstructed face-capped pentagon	− 1.0466
	Book	− 1.0453
	Chair	− 1.0000
	Corner-capped pentagon	− 0.9995
7	One face three-capped trigonal pyramid	− 1.1265
	Edge-capped book	− 1.1209
	Square edge shared with a pentagon	− 1.0899
	Corner-capped book	− 1.0308
8	Cube	− 1.2402
	Two edge-shared pentagons	− 1.1243
	Corner-c. pentagon edge s. with square	− 1.0778
	Bicorner-capped pentagon	− 0.9997
9	Face-capped cube	− 1.2710
10	Two stacked pentagons	− 1.3208
11	Edge capped two stacked pentagons	− 1.3414
12	Ground state [Fig. 1(j)]	− 1.3764
13	Ground state [Fig. 1(k)]	− 1.3894
14	Ground state [Fig. 1(l)]	− 1.4168

this definition, we calculated $g(r)$ for each individual cluster size at the temperatures 4 and 300 K, respectively. At low temperature, the clusters still remain in the ground-state configuration, so as we already know these structures, the interpretation of the curves at $T = 4$ K in Figs. 17–19 is straightforward. For small N ($N < 6$), the number of distinct structures is small and the structures are well separated in energy (see Fig. 4). At higher T the peaks in $g(r)$ broaden but the over all number of peaks remain the same as at $T = 4$ K. For $N > 6$ the number of structures begins to be large and often the structures are close in energy (for instance, we found around 150 structures on an energy range of 0.15 ϵ for $N = 14$). Clearly as T is increased these structures which are close in energy can transform from one to another resulting in a different sort of broadening in $g(r)$ in that each peak has contributions from several structures.

In the experimental situation, even if it were possible to generate a beam constituting of only one cluster size, the fragmentation process would create, in fact, a beam in which several sizes would be present. Therefore, to obtain the pair-distribution function corresponding to a real experimental situation we assume that each individual cluster will contribute to $g(r)$ with the distribution of probability $f(N)$ found in the photofragmentation study on Ge. Then the global pair-distribution function, less normalization constants, will be proportional to

$$G(r) = \frac{\Sigma_N f(N) g_N(r)}{\Sigma_N f(N)}, \tag{10}$$

where $g_N(r)$ is the individual pair-distribution function for each cluster of N atoms and $f(N)$ is its distribution probability. Figure 20 gives the result of these calculations showing at $T = 4$ K a predominance of squares (the peak at 1.65 σ corresponds to the diagonal of the square), distorted pentagons (characteristic of Ge_6 ground state) and pentagons. This was expected since the most significant contribution for $G(r)$ comes from Ge_6 and Ge_{10}, which are built mainly by those units. At 300 K, due to the proximity of those peaks the thermal effect makes them overlap giving to $G(r)$ the liquid-like characteristic with only the first peak clearly identifiable.

VI. MAGIC NUMBERS

Since it is possible to superheat clusters, the fragmentation energy was determined by heating or cooling several systems at energies near fragmentation. In this way, more than 50 systems were generated and about 20 fragmentations were observed for each cluster size. From the systems which remained bound for at least 25 000 Δt we took the one with the highest energy and defined it as the fragmentation energy. We also defined a fragmentation temperature T_f given by averaging the kinetic energy for that system. Figure 21 shows E_f and T_f as a function of clusters sizes. Since our preliminary results indicated that $N = 14$ is a magic number, we also studied the fragmentation of clusters with $N = 15$ and 16 atoms. It was found that the fragmentation energy and temperature of Ge_{14} is greater than its neighbors.

From Fig. 21 it is evident that $N = 10$ and 14 are more stable than their neighbors. For $N = 6$ the evidence is not so clear because the differences in fragmentation energy and temperature of $N = 6$ and 7 are within statistical fluctuations. However, it is clear that Ge_5 fragments more easily than Ge_6.

If we look at the structures at high energies, a possible explanation for the greater stability of $N = 6$ and 10 can be given noting that the most common structures at 0.95 E for these clusters contain a single bonded atom or a chain corner capped to a pentagon. In this particular arrangement the corner-capped atom sees its neighbors as if it were in a chain and the chains are structures in which the possibility of vibration are the greatest so, they can remain bound at greater internal temperatures.

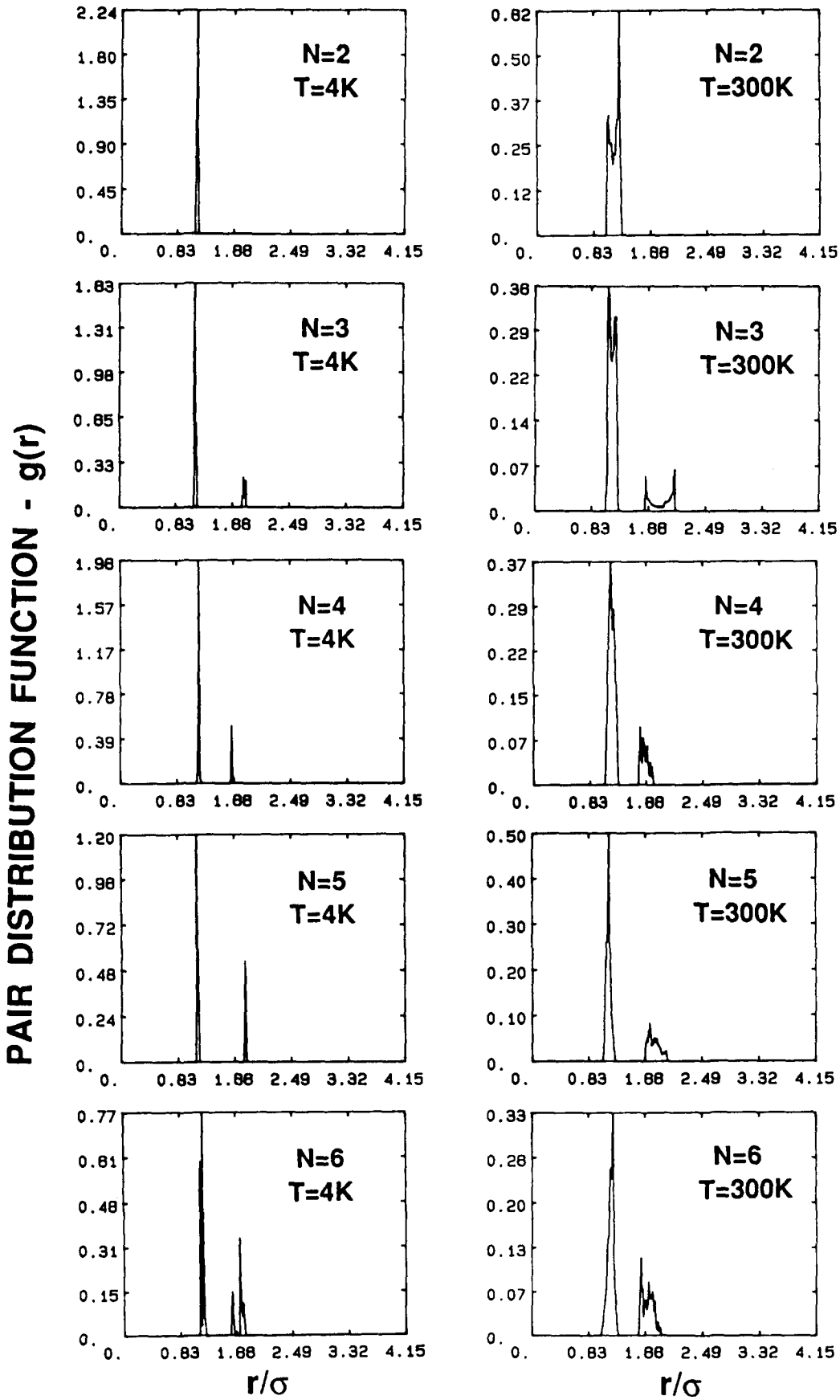

FIG. 17. Pair distribution function $g(r)$ for individual clusters at two temperatures, 4 and 300 K, respectively. (a) $N=2$, $T=4$ K; (b) $N=2$, $T=300$ K; (c) $N=3$, $T=4$ K; (d) $N=3$, $T=300$ K; (e) $N=4$, $T=4$ K; (f) $N=4$, $T=300$ K; (g) $N=5$, $T=4$ K; (h) $N=5$, $T=300$ K; (i) $N=6$, $T=4$ K; (j) $N=6$, $T=300$ K.

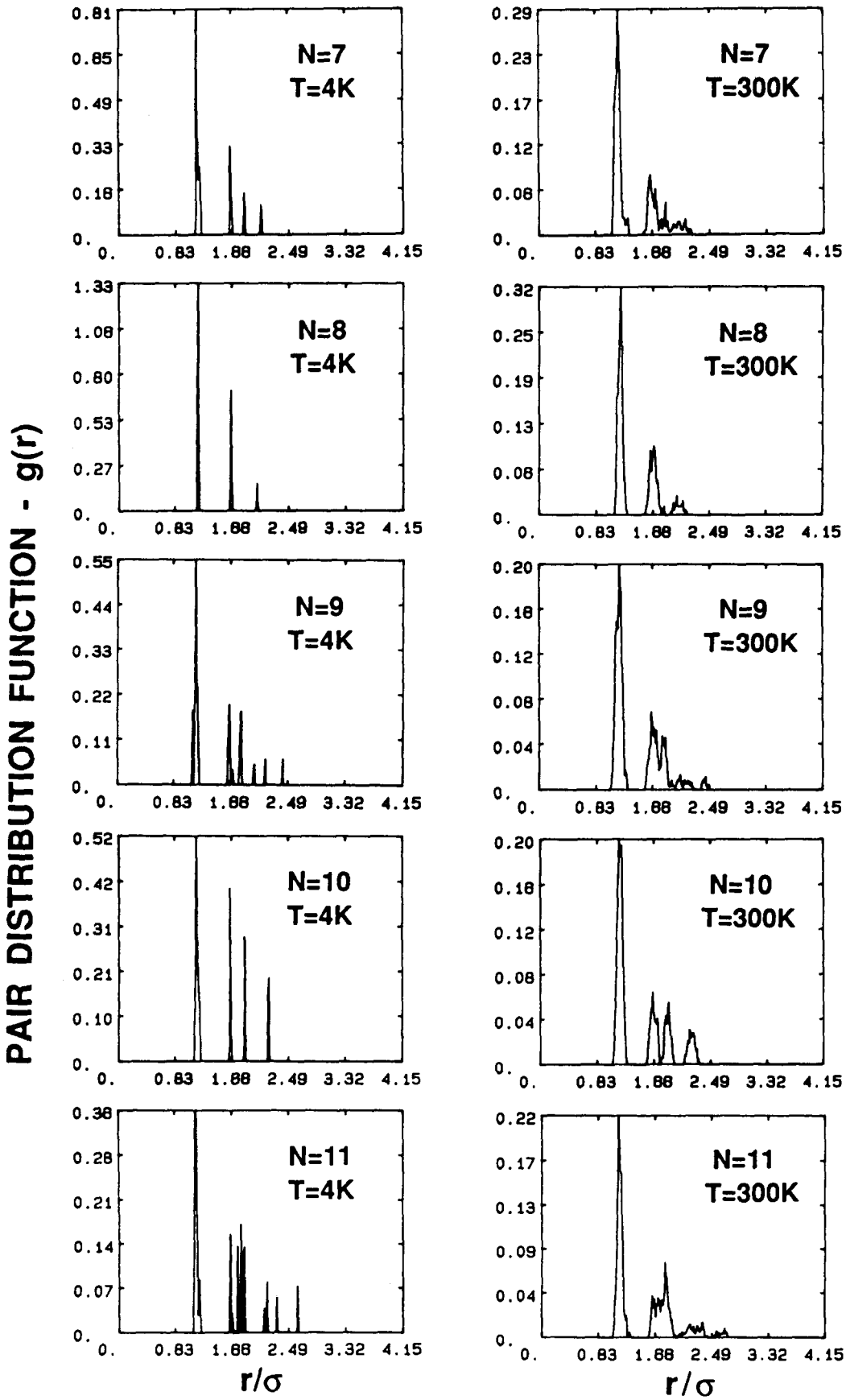

FIG. 18. Pair distribution function $g(r)$ for individual clusters at two temperatures, 4 and 300 K, respectively. (a) $N=7$, $T=4$ K; (b) $N=7$, $T=300$ K; (c) $N=8$, $T=4$ K; (d) $N=8$, $T=300$ K; (e) $N=9$, $T=4$ K; (f) $N=9$, $T=300$ K; (g) $N=10$, $T=4$ K; (h) $N=10$, $T=300$ K; (i) $N=11$, $T=4$ K; (j) $N=11$, $T=300$ K.

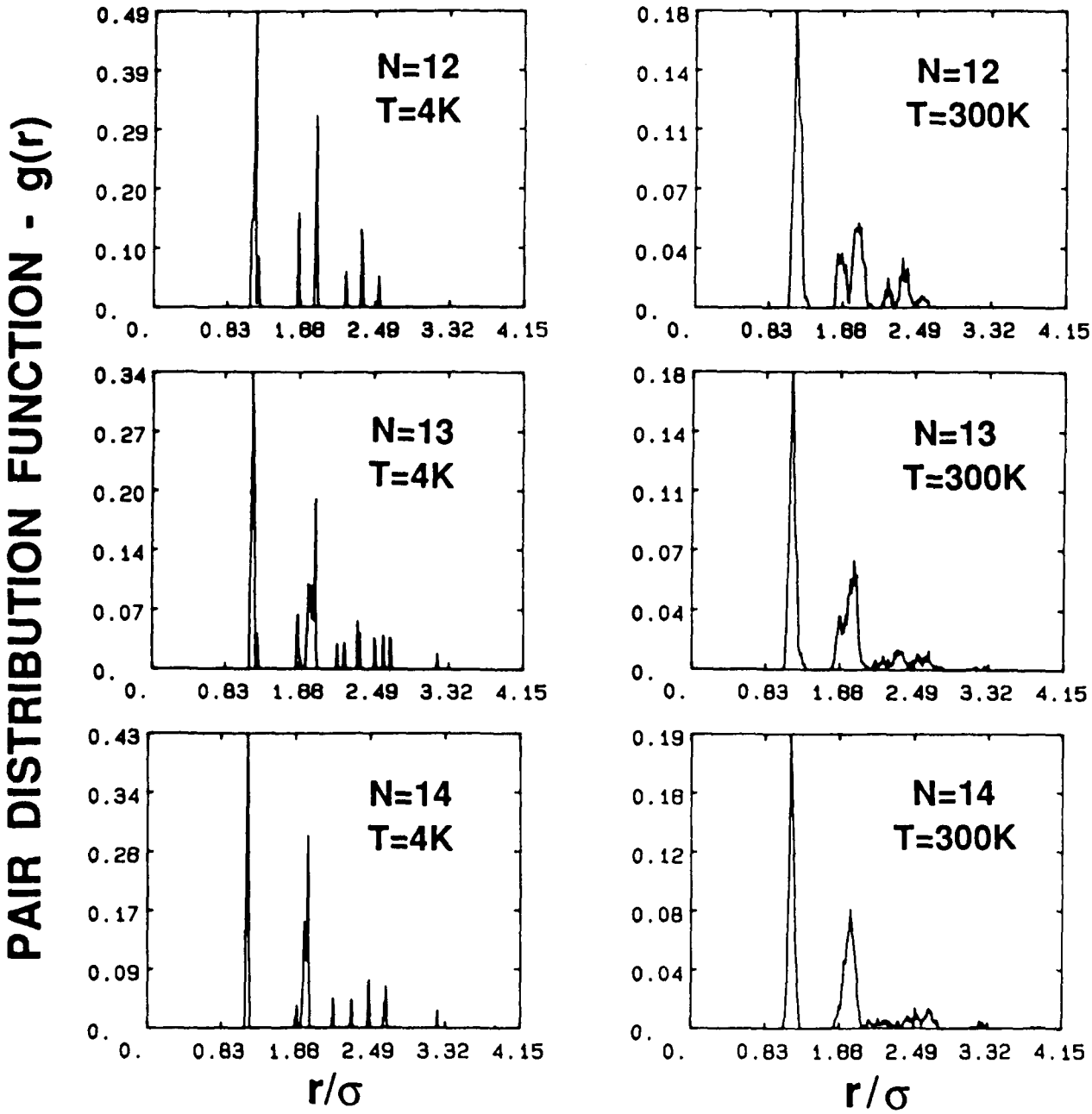

FIG. 19. Pair distribution function $g(r)$ for individual clusters at two temperatures, 4 and 300 K, respectively. (a) $N=12$, $T=4$ K; (b) $N=12$, $T=300$ K; (c) $N=13$, $T=4$ K; (d) $N=13$, $T=300$ K; (e) $N=14$, $T=4$ K; (f) $N=14$, $T=300$ K.

Table III shows the calculated probability of dissociation of each cluster size, $N \rightarrow (N-i)+i(i=1-6)$, from the observed fragmentations. In general, a cluster with N atoms prefers to dissociate into a $N-1$ cluster plus one atom. The only exception is Ge_4, which prefers to dissociate into two dimers. This can be explained by the fact that near fragmentation the most common underlying structure ($\approx 75\%$) for Ge_4 is the chain, for which it is easier to break the most rigid bond instead of the end bonds.

There are two possibilities to explain the greater stability of one given cluster size in the photofragmentation experiment. Either the cluster is more stable and does not fragment at all or it is a result of fragmentation of a larger cluster. The first argument is useful in explaining that 4, 6, and 10 are clusters more stable than the others, since their rate of fragmentation into $(N-1)+1$ atoms is smaller. In the case of Ge_4 also the fragmentation of Ge_5, Ge_6, and Ge_7 indicate that four may be a magic number for Ge. The dominance of Ge_{14} can be explained by the high rate of dissociation of Ge_{16} into $(N-2)+2$.

Our results for the magic numbers compare favorably with the experimental magic numbers found by Bloomfield *et al.* ($N=6$ and 10) and Martin and Schaber (6, 10, 14, 15, and 18).

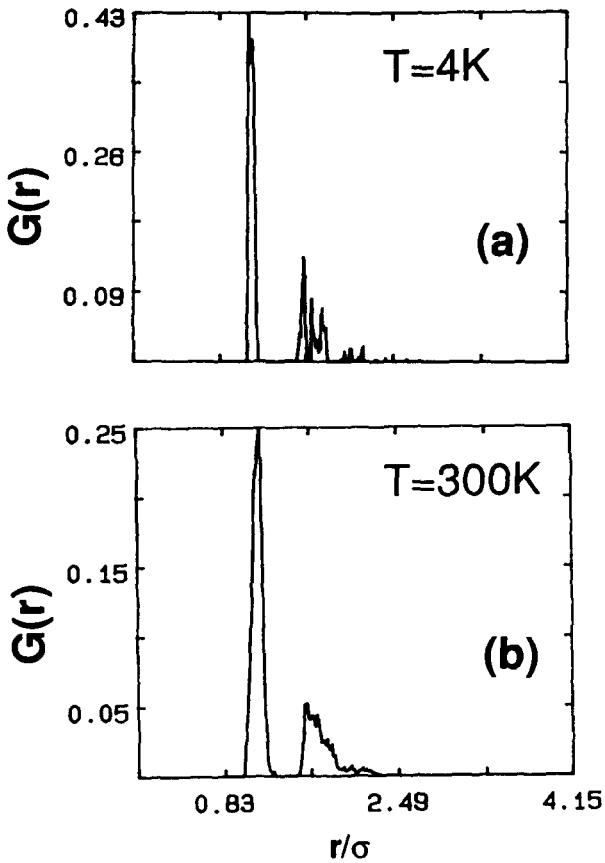

FIG. 20. These curves are the result of a weighted sum of $g(r)$ for the individual clusters. The weight factors were taken from the relative intensity of the peaks in the photofragmentation experiment of Bloomfield *et al.* for Ge.

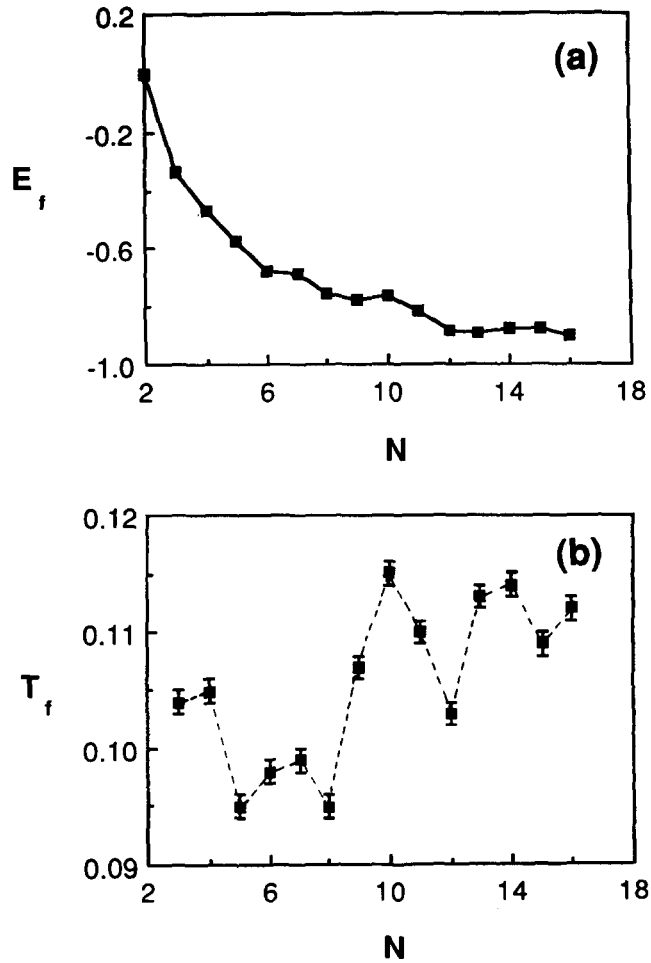

FIG. 21. (a) Fragmentation energy E_f vs cluster size and (b) fragmentation temperature T_f vs cluster size. The fragmentation energy E_f is defined by the system with the highest energy which does not fragment in a MD run of 25 000 Δt. T_f is the average temperature of the system with energy E_f.

This is to say that the magic numbers cannot be inferred by examining the $T = 0$ ground-state energies alone. Clearly the fragmentation is determined by the topology and energetics of the structures which are accessible to the systems near the fragmentation temperature.

VII. CONCLUSIONS

In this work we have shown that the geometries assumed by the clusters at energies near fragmentation are very different from that of the ground state and responsible for the difference of the abundance of different cluster sizes. The magic numbers, determined by looking for the highest energy in which a cluster does not fragment, agree in general with the experimental results, showing Ge_4, Ge_{10}, and Ge_{14} as more stable than the others. For Ge_6 the proximity with the fragmentation energy of Ge_7 does not permit a clear identification, however, there is a clear evidence that it is much more stable than Ge_5 (see Fig. 21).

The fragmentation channel observed to be in general $N \rightarrow (N-1) + 1$, has only the exception of Ge_4, which prefers to dissociate into dimers due to its particular structure at finite temperatures. The evaporation of an atom from the N cluster was also found in a recent work by Car, Parrinillo, and Andreoni, applying the simulated annealing technique for Si clusters ($N = 4$ and 5).

With the global pair-distribution function $G(r)$ calculated from the individual pair distribution function for each cluster size, we find it possible to identify, at low temperatures, at least the principal building blocks for Ge clusters (squares and pentagons) as well as the nearest neighbor distance.

TABLE III. Fragmentation channels for individual clusters. Cluster of size N fragmenting into $(N-i)+i$ for $i = 1$–6.

N	$(N-1)$	$(N-2)$	$(N-3)$	$(N-4)$	$(N-5)$	$(N-6)$
3	1.00					
4	0.35	0.65				
5	0.80	0.20				
6	0.59	0.41				
7	0.65	0.25	0.10			
8	0.75	0.20	0.05			
9	0.75	0.20	0.00	0.05		
10	0.62	0.24	0.09	0.05		
11	0.77	0.14	0.09	0.00		
12	0.75	0.15	0.00	0.10		
13	0.75	0.20	0.05	0.00		
14	0.75	0.20	0.00	0.00	0.05	
15	0.60	0.25	0.05	0.05	0.00	0.05
16	0.41	0.47	0.06	0.06	0.00	0.00

Since our calculations were done in reduced units we can also consider these results as for the Si case with $\lambda = 31$. From this point of view, we can qualitatively say that the increase of λ in the SW potential will affect most profoundly those structures which are formed by equilateral triangles where the deviation from tetrahedral angles is large. So as λ is increased, the general trend is that the overall percentage of triangles will decrease whereas the structures with pentagonal components will increase.

Finally, when the experimental data for Ge clusters become available it will be possible, by fitting these data, to find a set of parameters specific for clusters. We believe that the Stillinger and Weber potential as modified by Ding and Andersen is able to give a good qualitative description of covalently bonded systems.

ACKNOWLEDGMENTS

One of the authors (G. A. A.) would like to acknowledge the financial support from CAPES (Post-Graduate Education Federal Agency-Brazil) and the hospitality of the Materials Science Division at Argonne National Laboratory.

[1]L. A. Bloomfield, R. R. Freeman, and W. L. Brown, Phys. Rev. Lett. **54**, 2246 (1985).
[2]J. R. Heath, Y. Liu, S. C. O'Brien, Q. Zhang, R. F. Curl, F. K. Tittel, and R. E. Smalley, J. Chem. Phys. **83**, 5520 (1985).
[3]T. P. Martin and H. Schaber, J. Chem. Phys. **83**, 855 (1985).
[4]J. C. Phillips, J. Chem. Phys. **85**, 5246 (1986).
[5]S. Saito, S. Ohnishi and S. Sugano, Phys. Rev. B **33**, 7036 (1986).
[6]R. J. Temkin, W. Paul and G. A. N. Connel, Adv. Phys. **22**, 581 (1973).
[7]G. Pacchioni and J. Koutecky, J. Chem. Phys. **84**, 3301 (1986).
[8]K. Raghavachari and V. Logovinsky, Phys. Rev. Lett. **55**, 2853 (1985).
[9]D. Tomanek and M. A. Schlüter, Phys. Rev. Lett. **56**, 1055 (1986).
[10]J. C. Phillips (to be published).
[11]W. L. Brown, R. R. Freeman, K. Raghavachari and M. Schluter, Science **235**, 860 (1987).
[12]P. N. Keating, Phys. Rev. **145**, 637 (1966).
[13]F. H. Stillinger and T. A. Weber, Phys. Rev. B **31**, 5262 (1985).
[14]J. Tersoff, Phys. Rev. Lett. **56**, 632 (1986).
[15]E. Pearson, T. Takai, T. Halicioglu, and W. A. Tiller, J. Cryst. Growth **70**, 33 (1984).
[16]R. Biswas and D. R. Hamann, Phys. Rev. Lett. **55**, 2001 (1985).
[17]E. Blaisten-Barojas and D. Levesque, Phys. Rev. B **34**, 3910 (1986).
[18]B. P. Feuston, R. K. Kalia, and P. Vashishta, Phys. Rev. B **35**, 6222 (1987).
[19]R. Car, M. Parrinello, and W. Andreoni, *Proceedings of the 1st NEC Symposium on Fundamental Approach to New Material Phases, Tokyo, Japan,* 1986 (in press).
[20]R. Car and M. Parrinello, Phys. Rev. Lett. **55**, 2471 (1985).
[21]W. Kohn and L. J. Sham, Phys. Rev. A **140**, 1133 (1965).
[22]K. Ding and H. C. Andersen, Phys. Rev. B **34**, 6987 (1986).
[23]D. Beeman, J. Comp. Phys. **20**, 130 (1976).
[24]E. A. Rohlfing, D. M. Cox, and A. Kaldor, J. Chem. Phys. **81**, 3322 (1984).
[25]W. Schulze, B. Winter, and I. Goldenfeld (to be published).
[26]J. Van de Walle and P. Joyes, Phys. Rev. B **32**, 8381 (1985).
[27]P. A. Montano, W. Schulze, B. Tesche, G. K. Shenoy, and T. I. Morrison, Phys. Rev. B **30**, 672 (1984).
[28]P. A. Montano, G. K. Shenoy, E. E. Alp, W. Schulze, and J. Urban, Phys. Rev. Lett. **56**, 2076 (1986).
[29]J. W. Lee and G. D. Stein, Surf. Sci. **156**, 112 (1985).
[30]J. Farges, M. F. de Feraudy, B. Raoult, and G.Torchet, Surf. Sci. **106**, 95 (1981).
[31]J. Farges, M. F. de Feraudy, B. Raoult, and G. Torchet, J. Chem. Phys. **78**, 5067 (1983).